

# Dayside Pc2 waves associated with flux transfer events in a 3D hybrid-Vlasov simulation

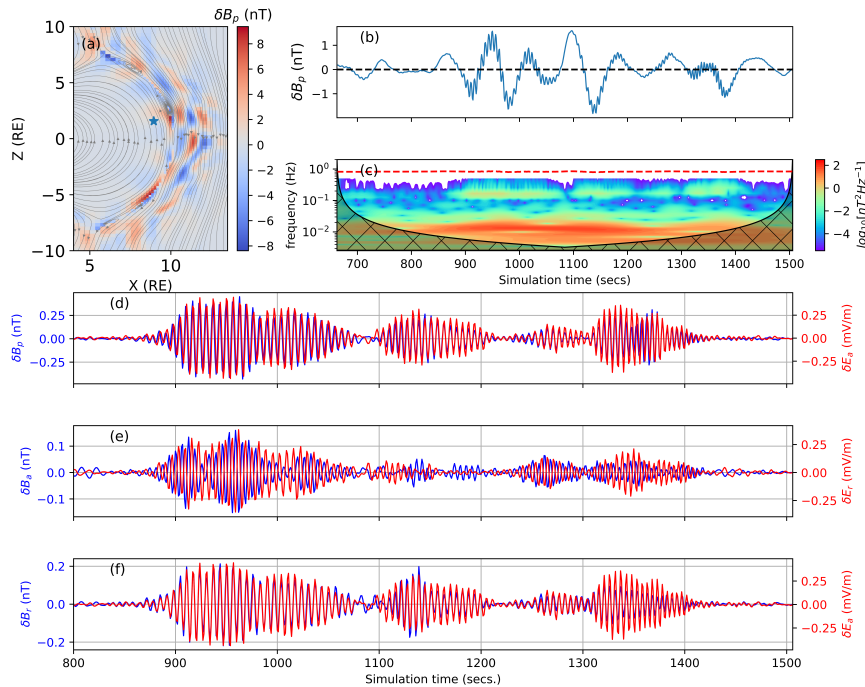
Fasil Tesema Kebede<sup>1</sup>, Minna Palmroth<sup>1</sup>, Lucile Turc<sup>1</sup>, Hongyang Zhou<sup>1</sup>, Giulia Cozzani<sup>1</sup>, Markku Alho<sup>1</sup>, Yann Pfau-Kempf<sup>1</sup>, Konstantinos Horaites<sup>1</sup>, Ivan Zaitsev<sup>1</sup>, Maxime Grandin<sup>1</sup>, Markus Battarbee<sup>1</sup>, Urs Ganse<sup>1</sup>, Abiyot Workayehu<sup>1</sup>, Jonas Emil Suni<sup>1</sup>, Konstantinos Papadakis<sup>1</sup>, Maxime Dubart<sup>1</sup>, and Vertti A Tarvus<sup>1</sup>

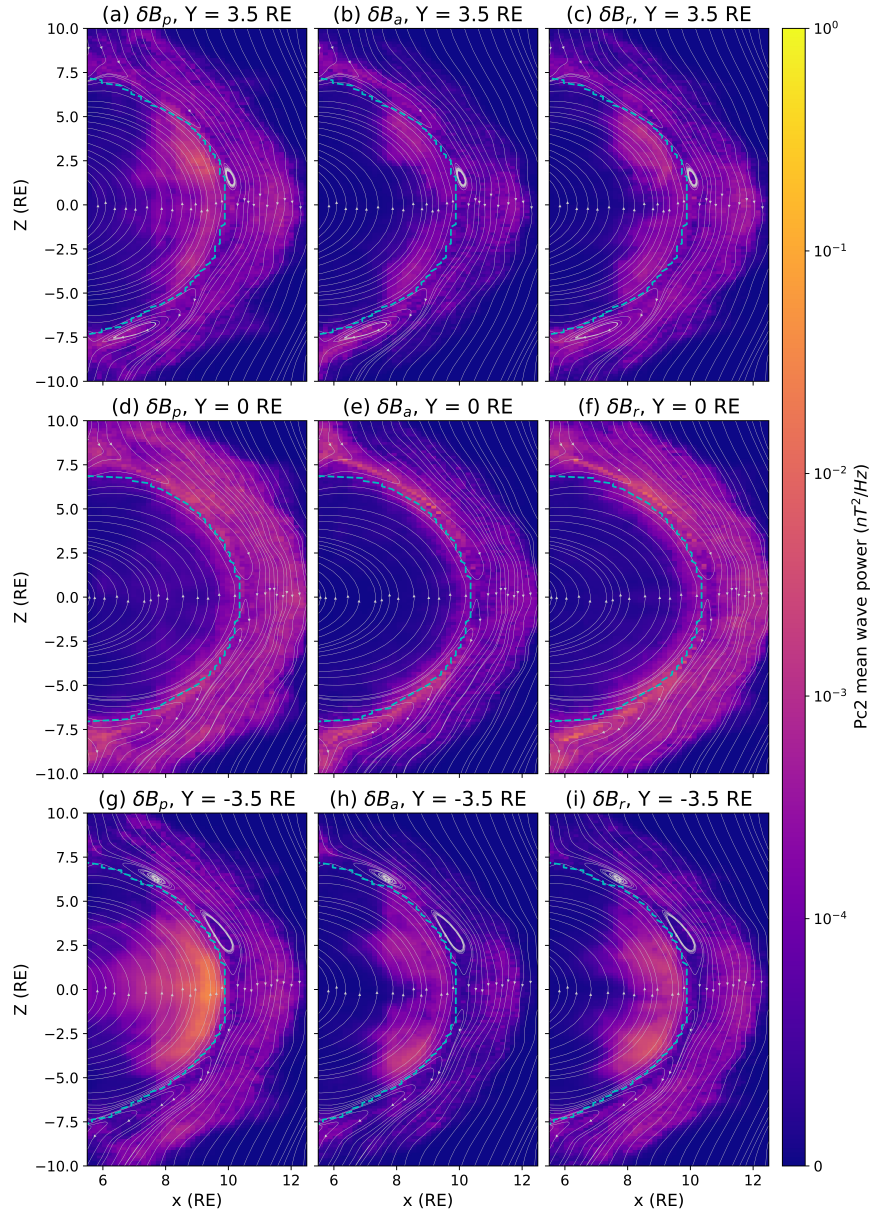
<sup>1</sup>University of Helsinki

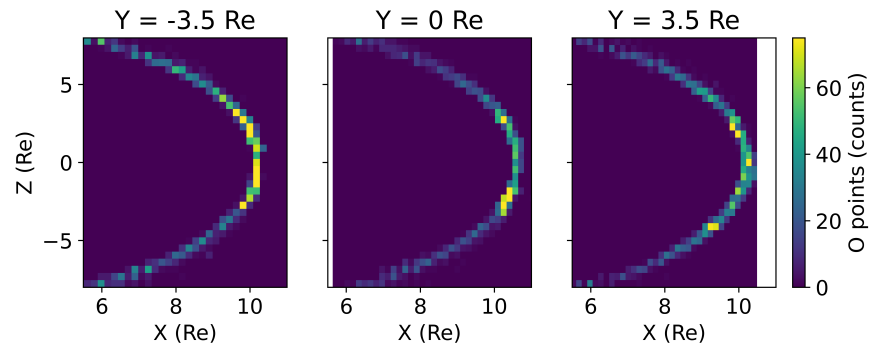
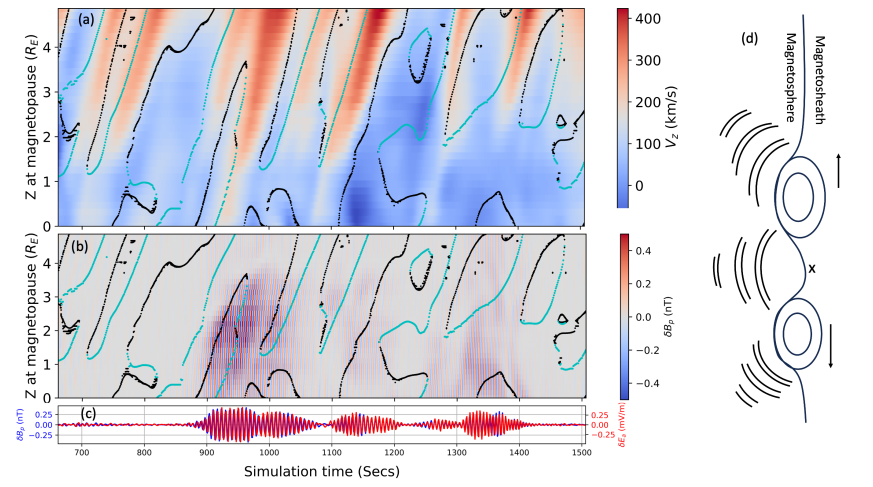
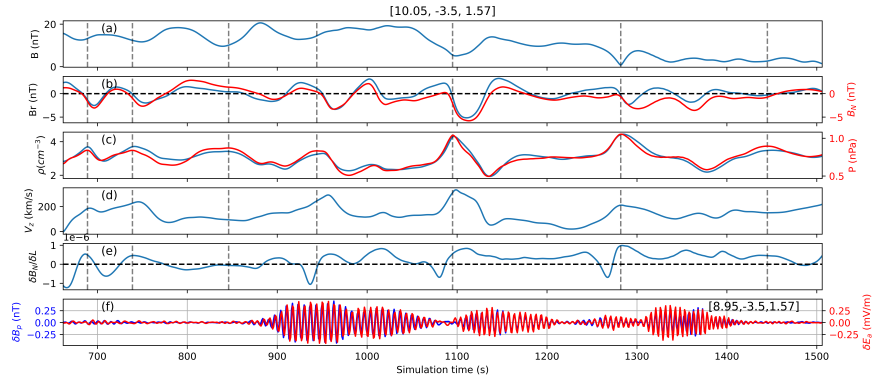
November 3, 2023

## Abstract

Flux transfer events (FTEs) are transient magnetic flux ropes at Earth’s dayside magnetopause formed due to magnetic reconnection. As they move across the magnetopause surface, they can generate disturbances in the ultra-low frequency (ULF) range, which then propagate into the magnetosphere. This study provides evidence of ULF waves in the Pc2 wave frequency range caused by FTEs during dayside reconnection using a global 3D hybrid-Vlasov simulation (Vlasiator). These waves resulted from FTE formation and propagation at the magnetopause are particularly associated with large, rapidly moving FTEs. The wave power is stronger in the morning than afternoon, showing local time asymmetry. In the pre and postnoon equatorial regions, significant poloidal and toroidal components are present alongside the compressional component. The noon sector, with fewer FTEs, has lower wave power and limited magnetospheric propagation.







# Dayside Pc2 waves associated with flux transfer events in a 3D hybrid-Vlasov simulation

F. Tesema<sup>1</sup>, M. Palmroth<sup>1,2</sup>, L. Turc<sup>1</sup>, H. Zhou<sup>1</sup>, G. Cozzani<sup>1</sup>, M. Alho<sup>1</sup>,  
Y. Pfau-Kempf<sup>1</sup>, K. Horaites<sup>1</sup>, I. Zaitsev<sup>1</sup>, M. Grandin<sup>1</sup>, M. Battarbee<sup>1</sup>,  
U. Ganse<sup>1</sup>, A. Workayehu<sup>1</sup>, J. Suni<sup>1</sup>, K. Papadakis<sup>1</sup>, M. Dubart<sup>1</sup>, V. Tarvus<sup>1</sup>

<sup>1</sup>Department of Physics, University of Helsinki, Helsinki, Finland

<sup>2</sup>Finnish Meteorological Institute, Space and Earth Observation Centre, Helsinki, Finland

## Key Points:

- Dayside Pc2 waves ( $> 0.1$  Hz) have been detected in a 3D hybrid-Vlasov simulation.
- These waves exhibit lower intensity within the magnetosphere at noon, compared to the prenoon and postnoon sectors.
- Pc2 waves observed in the simulation are associated with largest and fast moving flux transfer events initiated by subsolar reconnection.

**Abstract**

Flux transfer events (FTEs) are transient magnetic flux ropes at Earth's dayside magnetopause formed due to magnetic reconnection. As they move across the magnetopause surface, they can generate disturbances in the ultra-low frequency (ULF) range, which then propagate into the magnetosphere. This study provides evidence of ULF waves in the Pc2 wave frequency range caused by FTEs during dayside reconnection using a global 3D hybrid-Vlasov simulation (Vlasiator). These waves resulted from FTE formation and propagation at the magnetopause are particularly associated with large, rapidly moving FTEs. The wave power is stronger in the morning than afternoon, showing local time asymmetry. In the pre and postnoon equatorial regions, significant poloidal and toroidal components are present alongside the compressional component. The noon sector, with fewer FTEs, has lower wave power and limited magnetospheric propagation.

**Plain Language Summary**

The Earth's magnetosphere is a dynamic region shaped by the interplay between the solar wind and Earth's magnetic field. This interaction occurs at the boundary of the magnetosphere (magnetopause) through a process known as magnetic reconnection, giving rise to Flux Transfer Events (FTEs), which are magnetic structures that carry flux and energy into the magnetosphere. These FTEs form either in sudden bursts, patchy patterns or in a continuous, and relatively stable way making the magnetopause surface dynamic. As the FTEs move along the boundary of the magnetosphere, they create compressed regions and lead to wave generation that can extend into the magnetosphere. The study uses an advanced 3D hybrid-Vlasov simulation model to analyze waves originated from FTE formation and propagation at the magnetopause. We find that rapidly moving and large FTEs have a significant impact on the magnetopause, leading to the generation of ULF waves with frequency above 0.1 Hz. This shows first direct evidence supporting previous theoretical speculations regarding the ability of FTEs to generate waves near the magnetopause.

**1 Introduction**

Ultra low-frequency (ULF) waves in the Earth's magnetosphere play a crucial role in shaping the dynamics of radiation belts (Zong et al., 2017; Ripoll et al., 2020). The global occurrence and spatial distribution of these waves have captured considerable attention due to their role in transport and couple energy between solar wind and magnetosphere, energisation and loss of radiation belt particles (Menk et al., 2011). The literature extensively covers the generation mechanisms of ULF waves, which are primarily linked to fluctuations in the solar wind on the dayside, including pressure pulses and Kelvin-Helmholtz instability, as well as magnetospheric processes, such as substorms and other instabilities occurring on the nightside in the magnetotail (McPherron, 2005; Hwang & Sibeck, 2016; Bentley et al., 2018).

Numerous studies have proposed that the formation and propagation of flux transfer events (FTEs) along the surface of the magnetopause could compress the magnetic field and launch ULF waves in the Pc3 to Pc5 range (100–500 seconds) into the magnetosphere (Russell & Elphic, 1979; Glasmeier et al., 1984; Gillis et al., 1987; J. Liu et al., 2008; Bentley et al., 2018). This could arise due to the energy conversion related to magnetopause reconnection and the draping of magnetic field lines by FTEs along the magnetopause's surface (Arnoldy et al., 1988; Yagodkina & Vorobjev, 1997; Hwang, 2015). Furthermore, when the resulting quasi-periodic perturbations in the Pc3 to Pc5 range reach a sufficient magnitude, the FTE-generated compressional fast mode waves can propagate into the magnetosphere, and ultimately give rise to inner magnetospheric waves (Russell & Elphic, 1979; Gillis et al., 1987; Hwang & Sibeck, 2016).

Several studies have demonstrated that dayside reconnection can occur in either bursty and patchy patterns or in a continuous or quasi-steady manner with multiple reconnection points or separator lines occurring sequentially (e.g. Hasegawa et al., 2006, 2010; Fear et al., 2008; Tan et al., 2011; Hoilijoki et al., 2017; Walsh et al., 2017; H. Wang et al., 2019; Pfau-Kempf et al., 2020; Trattner et al., 2021). This deforms the magnetopause, creating recurring FTEs that are often accompanied by ULF pulsations at the magnetopause (Yagodkina & Vorobjev, 1997). Measurements from off-equatorial magnetospheric regions (Y. H. Liu et al., 2012) and research based on indirect observations (Kokubun et al., 1988; Arnoldy et al., 1988; Yagodkina & Vorobjev, 1997) have speculated that FTEs could also generate waves in the Pc1-2 frequency range. However, the direct link between waves in the frequency range above Pc3 and FTEs has not been made. This paper establishes the first direct link between Pc2 waves and the propagation and formation of FTEs on the dayside, utilizing a 3D hybrid-Vlasov simulation.

## 2 Model

In this study, we used the Vlasiator simulation (Palmroth et al., 2023), a global hybrid-Vlasov model described in Von Althaus et al. (2014), Palmroth et al. (2018), and Ganse et al. (2023). Vlasiator self-consistently models the global ion dynamics using a 6D phase space (3D in physical space and 3D in velocity space) while electrons are treated as a charge-neutralizing fluid. The Ohm's law includes the convective, Hall, and electron pressure terms assuming an adiabatic electron fluid. Further implementation details of Vlasiator can be found in Palmroth et al. (2018).

The simulation was carried out in a domain defined by the boundaries  $x = [-110.5, 50.2]R_E$ ,  $y = [-57.8, 57.8]R_E$ ,  $z = [-57.8, 57.8]R_E$ , with  $R_E$  corresponding to the Earth's radius of 6371 km, encompassing the near-Earth solar wind, the dayside magnetosphere and an extended magnetotail and based on Geocentric Solar Ecliptic (GSE) coordinate system. The inner boundary was a near-ideal conducting sphere at a distance of  $4.7 R_E$ , and the simulation employed adaptive mesh refinement (AMR) with three levels of spatial resolution, the highest resolution ( $0.16 R_E$ ) around the magnetopause and magnetotail current sheet (Ganse et al., 2023). The simulation setup incorporated constant and homogeneous solar wind conditions, with the solar wind velocity of  $750 \text{ km s}^{-1}$  along the -x direction, a purely southward interplanetary magnetic field of 5 nT, a solar wind density of  $n_{sw} = 1 \text{ cm}^{-3}$ , a solar wind temperature of  $T_{sw} = 5 \times 10^5 \text{ K}$ , and an Alfvénic Mach number of  $M = 6.9$ .

Vlasiator's capability to resolve kinetic physics in detail results, among others, in its capability to reproduce the velocity distribution function in detail, as many of the kinetic physics and waves arise from the higher energy populations that are well resolved both in space and in velocity space (see Palmroth et al., 2023). Vlasiator has been shown to capture various ion kinetic phenomena (Hoilijoki et al., 2017; Pfau-Kempf et al., 2018, 2020). Additionally, several studies have validated their findings from Vlasiator using satellite observations (e.g. Palmroth et al., 2015; Pfau-Kempf et al., 2016; Akhavan-Tafti et al., 2020; Palmroth et al., 2021; Takahashi et al., 2021; Grandin et al., 2023).

## 3 Results

In this section, we present findings from the simulation described above, conducted for a duration of 1506 seconds. Our analysis considers data collected after the initialization phase, 662 seconds of the simulation. To characterize Pc2 waves in the simulation, we remove the background magnetic field by subtracting a moving average calculated over an interval much longer than the period of the ULF waves of interest. In this work we are interested in the frequency range above 0.1 Hz. Thus, the window for the moving average is set to 100 seconds, which can also capture ULF waves with frequencies down to 0.006 Hz including those in the Pc4 range. We denote this magnetic field

114 variation vector, with the background subtracted, as  $\delta\mathbf{B}$ . All field parameters are trans-  
 115 formed into local magnetic field-aligned coordinates (FAC) following the method out-  
 116 lined in Regi et al. (2017). The FAC system has three axes: one axis aligned with the  
 117 local magnetic field direction ( $\delta B_p$ ) and two axes perpendicular to it, along the radial  
 118 ( $\delta B_r$ ) and azimuthal directions ( $\delta B_a$ ). In addition to the FAC system we also used the  
 119 LMN coordinate system and the contouring method described in Alho et al. (2023) to  
 120 identify FTE axes and their distributions. In this coordinate system L is along the max-  
 121 imum local variation of the magnetic field, N is orthogonal to L and approximately nor-  
 122 mal to the magnetopause current sheet, and M completes the right-handed orthonormal  
 123 system. We also used the gradient of the normal magnetic field around the magnetopause  
 124 as a proxy to determine the size of FTEs.

### 125 3.1 ULF waves near the magnetopause

126 To investigate the generation of Pc2 waves near passing FTEs, in Figure 1 we present  
 127 a case study involving a virtual satellite situated at coordinates  $[x = 8.95, y = -3.5, z =$   
 128  $1.57]R_E$  within the magnetosphere (indicated by a blue star). This virtual satellite ob-  
 129 serves magnetic field pulsations, and Figure 1 (b) and (c) depict the variations of the par-  
 130 allel magnetic field component ( $\delta B_p$ ) and its wavelet power spectrum calculated using  
 131 Morlet wavelet (Torrence & Compo, 1998). The wavelet power spectrum shows enhanced  
 132 wave power in two distinct frequency bands: one localized in the frequency range between  
 133 0.1–0.3 Hz with a peak of 0.125 Hz (corresponding to Pc2 waves with an 8-second pe-  
 134 riod), and another between 5–20 mHz with a peak at 10 mHz, corresponding to Pc4 waves.  
 135 Our focus in this study is on the Pc2 waves. We also present a movie of these waves on  
 136 three planes which are associated with prenoon, noon and postnoon periods (see Movie  
 137 S1 in supplementary information). In the movie, Pc2 waves represented by  $\delta B_p$  are shown  
 138 on planes at  $y = 3.5R_E$  (postnoon),  $y = 0R_E$  (noon), and  $y = -3.5R_E$ . The waves  
 139 are originated from the magnetopause and propagating into the magnetosphere, and are  
 140 more prominent in the post and prenoon planes.

141 In the Earth’s magnetosphere, ULF waves typically exhibit a combination of polar-  
 142 izations, including compressional, toroidal, and poloidal modes (Lee & Lysak, 1989;  
 143 McPherron, 2005). Figure 1 (d-f) displays the three polarization components (compres-  
 144 sional, toroidal, and poloidal) after filtering using a 5th order band-pass Butterworth fil-  
 145 ter within the frequency range of [0.1–0.5] Hz. The poloidal mode involves radial mag-  
 146 netic field pulsations and azimuthal electric field fluctuations, while the toroidal mode  
 147 features variations in azimuthal magnetic field and radial electric field. The compressional  
 148 mode is associated with oscillations mainly in the parallel magnetic field component and  
 149 azimuthal electric field. Notably, there is significant interaction between compressional  
 150 and poloidal oscillations, as both involve field line oscillations in the radial direction (Lee  
 151 & Lysak, 1989). From all the three panels, starting around 870 seconds into the simu-  
 152 lation, significant pulsation amplitudes occur periodically. The compressional compo-  
 153 nent exhibits the highest amplitude, reaching up to  $|\delta B_p| = 0.45$  nT,  $|\delta E_a| = 0.44$  mV/m,  
 154 while the poloidal and toroidal components have maximum amplitudes of  $|\delta B_r| = 0.21$   
 155 nT,  $|\delta E_r| = 0.38$  mV/m and  $|\delta B_a| = 0.16$  nT,  $|\delta E_a| = 0.44$  mV/m, respectively. No-  
 156 tably, the compressional and poloidal components feature three distinct wave packets dur-  
 157 ing the time intervals of 870–1070, 1100–1200, 1200–1300, and 1300–1400 seconds.

158 To further investigate the spatial distribution of Pc2 waves depicted in Figure 1  
 159 (c), Figure 2 presents the distribution of wave power, averaged over the higher frequency  
 160 band ([0.1–0.5] Hz) with a similar approach used in Turc, Zhou, et al. (2022). This dis-  
 161 tribution is shown across three distinct planes in the dayside magnetosphere, with data  
 162 collected after 800 seconds into the simulation when Pc2 waves first become apparent  
 163 in the magnetosphere. The three polarization components ( $\delta B_p$ ,  $\delta B_a$ , and  $\delta B_r$ ) were ex-  
 164 tracted from planes at  $y = 3.5R_E$  (postnoon),  $y = 0R_E$  (noon), and  $y = -3.5R_E$   
 165 (prenoon). In the magnetosheath, the noon sector exhibits considerably higher compres-

166 sional and poloidal mean wave power than the other sectors. In contrast, within the mag-  
 167 netosphere, the prenoon sector shows the highest values for all polarization components,  
 168 followed by the postnoon sector. Compressional wave modes dominate over toroidal and  
 169 poloidal Pc2 ULF waves in the pre- and postnoon sectors, with the latter showing lower  
 170 wave power, as demonstrated in Figure 2(b), (c), (h), and (i). The poloidal and toroidal  
 171 modes were not detected deep within the magnetosphere near the magnetospheric equa-  
 172 torial plane. Additionally, the mean wave power significantly decreases as we go towards  
 173 the cusp in both hemispheres. Despite the higher values of all components in the noon  
 174 sector of the magnetosheath, the noon sector within the magnetosphere lacks significant  
 175 wave power. Overall, the poloidal and toroidal components are restricted within the re-  
 176 gion between magnetopause and  $x = 8R_E$ , however, the compressional mode is seen  
 177 beyond  $x = 8R_E$  into the magnetosphere, especially in the prenoon sector ( $Y = -3.5R_E$   
 178 plane).

### 179 3.2 Origin of Pc2 waves

180 To investigate the origin of the Pc2 waves depicted in Figure 2, in Figure 3 we demon-  
 181 strate a correspondence between the FTEs along the magnetopause surface and the waves.  
 182 We identified FTEs at a virtual spacecraft location approximately one Earth radius away  
 183 in the x direction from where the waves are depicted in Figure 1(a) (blue star), near the  
 184 magnetopause surface at coordinates  $[x = 10.05, y = -3.5, z = 1.57]R_E$ . FTEs are  
 185 typically recognized by the presence of a bipolar variation in the magnetic field compo-  
 186 nent that is locally perpendicular to the magnetopause (Russell & Elphic, 1979; Paschmann  
 187 et al., 1982). However, additional indicators, such as an increase in magnetic field strength  
 188 on the magnetosheath side of the FTE or a decrease on the magnetosphere side, elevated  
 189 total pressure, and an increase in plasma bulk velocity in the z direction, have also been  
 190 used to identify FTEs (Paschmann et al., 1982; Zhang et al., 2011; Teh et al., 2017; Sun  
 191 et al., 2019).

192 In Figure 3(a-d), the combination of the FTE-related parameters, including the mag-  
 193 netic field magnitude, the radial and normal components of the magnetic field, plasma  
 194 density and pressure, the z-component of plasma velocity, and the derivative of the lo-  
 195 cal normal magnetic field along the  $L$  direction are used to indicate the presence of FTEs  
 196 (marked with vertical dashed lines). The variations in magnetic field magnitude, the bipo-  
 197 larity of  $B_r$  and  $B_N$ , along with peak pressure and density, collectively suggest the ex-  
 198 istence of FTEs. In panel (e) of this figure, we present the gradient of  $B_N$  along the lo-  
 199 cal magnetic field direction ( $L$ ) to indirectly infer the size of the passing FTE. The sig-  
 200 nificant variation and bipolarity of this gradient, after 900 seconds, around 1100 seconds,  
 201 and before 1300 seconds, are observed near the wave packets shown in the last panel of  
 202 the Figure 3, indicating the presence of large FTEs passing by.

203 Upon comparing Figure 3 (f) with the supplementary Movie S1, it becomes evi-  
 204 dent that FTEs, as they move along the magnetopause surface, give rise to the Pc2 waves.  
 205 These waves are initiated during FTEs characterized by a significantly higher z-direction  
 206 plasma bulk velocity (panel (d)) and are notably absent when the velocity drops below  
 207 100 km/s. This distinction is particularly pronounced before the 900-second mark and  
 208 during the period between 1200 and 1300 seconds. In addition, a visual comparison of  
 209 FTE occurrences, distribution of O points from (Alho et al., 2023) method, in the three  
 210 planes presented in the supplementary Figure S1 reveals a significant difference between  
 211 the  $Y = -3.5R_E$  and  $Y = 3.5R_E$  planes when compared to the noon-midnight plane.  
 212 This occurrence pattern mirrors the Pc2 wave power illustrated in Figure 2. The ma-  
 213 jority of FTE formations are localized within the range of  $Z = \pm 4R_E$  on the three planes  
 214 (refer to the supplementary information video).

215 In Figure 4, we further illustrate the link between the FTE motion and the wave  
 216 patterns presented on the plane  $Y = -3.5R_E$  (see movie S1). Figure 4 (a) is a stacked

217 plot representing the z-component of plasma bulk velocity along the northern hemisphere  
 218 of the magnetopause surface. In panel (b) of this Figure we present the Pc2 wave stack  
 219 plot along a curve parallel to the magnetopause surface and inside the magnetosphere  
 220 that includes the blue star shown in Figure 1 (a). In addition, contour lines of X and O  
 221 points are superimposed as described in the Alho et al. (2023). Figure 4 (c) shows a sim-  
 222 ilar panel from Figure 1 (d).

223 Examining Figure 4 (b) and (c), we note that the first two wave packets observed  
 224 during the time periods 900–1060 and 1100–1200 in panel (c) are accompanied by re-  
 225 connection events (X points) occurring around the sub-solar point (within  $1R_E$ ), as well  
 226 as one or more FTEs occurring away from this region, which is clearly visible in Sup-  
 227plementary animation 1. The subsequent wave packet observed after 1300 seconds orig-  
 228 inates from the reconnection region, as no O points are observed during this time pe-  
 229 riod and around the sub-solar point. It is also worth highlighting that the time periods  
 230 before 750 seconds and after 1400 seconds lack X points around the sub-solar point. To  
 231 provide a schematic illustrating the scenario we propose to explain the observations throug-  
 232 hout the entire simulation, we have included a schematic representation in Figure 4 (d).  
 233 This illustration shows three source regions: one at the leading edge of the diverging FTEs,  
 234 another at the reconnection region, and potentially the trailing edge of the two FTEs.  
 235 During the entire simulation period (see Movie S1), the Pc2 waves observed originate  
 236 from either of these three sources or a combination thereof.

## 237 4 Discussion

238 In this study, we have shown direct evidence of a previously speculated source of  
 239 Pc2 waves which are associated with the formation and passage of FTEs along the mag-  
 240 netopause surface. Using a hybrid-Vlasov simulation, we demonstrated that these waves  
 241 exhibit large wave power in the compressional, toroidal, and poloidal components with  
 242 the compressional component being notably more dominant near the magnetospheric equa-  
 243 tor in close proximity to the magnetopause. Furthermore, we establish a strong connec-  
 244 tion between the presence of Pc2 waves and the occurrence of large, high-velocity FTEs  
 245 initiated through a sub-solar reconnection.

246 In our simulation, despite the steady southward IMF, the reconnection process ap-  
 247 pears to be dynamic, as previously reported in 2D and 3D hybrid-Vlasov simulations by  
 248 Hoilijoki et al. (2017) and Pfau-Kempf et al. (2020), as shown in Movie S1 of the sup-  
 249plementary information. Consequently, FTEs are continuously generated and propagate  
 250 along the magnetopause. It is important to note that all the solar wind parameters re-  
 251 main constant throughout the simulation period, ruling out the possibility of attribut-  
 252 ing the Pc2 waves observed in our study to solar wind variations (Usanova et al., 2012).  
 253 While Kelvin-Helmholtz instability (KHI) can also generate ULF waves, their efficiency  
 254 and persistence are notably enhanced when the IMF orientation is northward (Hwang,  
 255 2015; Kavosi & Raeder, 2015), which is not the case in our simulation. KHI also exist  
 256 during southward IMF, however, they are thought to drive Pc4-5 waves (C. P. Wang et  
 257 al., 2017; Kronberg et al., 2021). In addition, the process of ULF waves originating from  
 258 foreshock-generated sources and propagating across the magnetopause (Turc, Roberts,  
 259 et al., 2022) is excluded due to the strictly southward orientation of the IMF, prevent-  
 260 ing the formation of the foreshock in front of the magnetopause nose. Thus, we conclude  
 261 that the origin of the observed waves in the vicinity of the magnetopause in our simu-  
 262 lation is attributed to magnetic reconnection and FTE propagation at the magnetopause  
 263 surface. We have also clearly demonstrated this direct connection between FTEs and their  
 264 propagation during active sub-solar reconnection.

265 Using spectral analysis of magnetic field component fluctuations, we have demon-  
 266 strated that Pc2 waves display significant wave power within a region of  $3R_E$  distance  
 267 from the magnetopause (Figure 2). In addition, we have observed that the wave power

268 in the magnetosphere is highest in the prenoon sector in all three polarization compo-  
 269 nents followed by the postnoon and noon sectors. Our simulation results indicate that  
 270 Pc2 waves have similar spatial distributions and magnetic local time (MLT) as those ob-  
 271 served in previous observational based studies (Grison et al., 2021). The MLT occurrence  
 272 of waves (between 0.1 and 2 Hz) in the vicinity of the magnetopause reported by Grison  
 273 et al. (2021) showed similar characteristics to what we observed in our simulation. Ad-  
 274 ditionally, Anderson et al. (1992) conducted a statistical analysis, revealing a higher oc-  
 275 currence rate of dayside Pc1-2 pulsations in the outer magnetosphere ( $L > 7$ ) compared  
 276 to the inner magnetosphere ( $L < 5$ ), coinciding with the same region where we observe  
 277 Pc2 waves in our simulation. FTE associated magnetic pulsations in the in 6 – 8 sec-  
 278 onds period (Pc2 range) of magnitude 0.1–0.2 nT is also reported by Yagodkina and  
 279 Vorobjev (1997).

280 The majority of investigations into ULF waves within the frequency range discussed  
 281 in this article (referred to as Pc2) have typically associated their driving mechanisms with  
 282 variations in solar wind parameters or temperature anisotropy resulting from the inter-  
 283 action between hot ions moving from the nighttime to the daytime side and the cold ions  
 284 in the plasmasphere (Usanova et al., 2012; Tetrick et al., 2017; Remya et al., 2018). How-  
 285 ever, this research also suggests that Pc2 waves may originate locally from the forma-  
 286 tion and propagation of Flux Transfer Events (FTEs). While this paper does not delve  
 287 into the processes underlying the formation and the most suitable model for describing  
 288 the FTEs observed in the simulation, Figure 4 and the accompanying video showcase  
 289 numerous instances of multiple reconnection X-lines. These X-lines are particularly preva-  
 290 lent in the region where high wave power was detected (Figure 4). Whether these recon-  
 291 nection sites or the motion of FTEs serve as the dominant sources of the waves remains  
 292 an unanswered question within the scope of this study, emphasizing the need for further  
 293 investigations.

## 294 5 Summary

295 This study utilizes a hybrid-Vlasov simulation to investigate dayside Pc2 waves in  
 296 the outer magnetosphere when a purely southward IMF and steady fast solar wind hits  
 297 the Earth’s magnetosphere. The study found Pc2 waves above 0.1 Hz frequency linked  
 298 to the formation and passage of FTEs across the dayside magnetopause. We established  
 299 a direct link between these waves and the presence of large, rapidly moving FTEs gen-  
 300 erated during sub-solar reconnection. Moreover, the study identified a significant asym-  
 301 metry in MLT wave power, with the prenoon sector exhibiting a greater dominance of  
 302 Pc2 waves compared to the noon and postnoon sectors. Substantial wave polarization  
 303 components in the poloidal and toroidal ULF modes were also detected in the off-equatorial  
 304 regions of the magnetosphere.

## 305 6 Open Research

306 The Vlasiator simulation code is freely available for download at <https://github.com/fmihpc/vlasiator>. To reproduce the data utilized in this study, refer to a con-  
 307 figuration file at Pfau-Kempf et al. (2022). The output of the simulation is stored in a  
 308 customized file format accessible at GitHub repository: <https://github.com/fmihpc/vlsv>. For post-processing of the simulation in this study a Python package, Analysator,  
 309 available at <https://github.com/fmihpc/analysator> (Battarbee et al., 2021) is used.  
 310  
 311

## 312 Acknowledgments

313 Vlasiator is developed by funding from the European Research Council Starting Grant  
 314 200141-QuESpace and Consolidator Grant 682068—PRESTISSIMO. We also appreci-  
 315 ate the support provided by the CSC-IT Center for Science in Finland and the Partner-

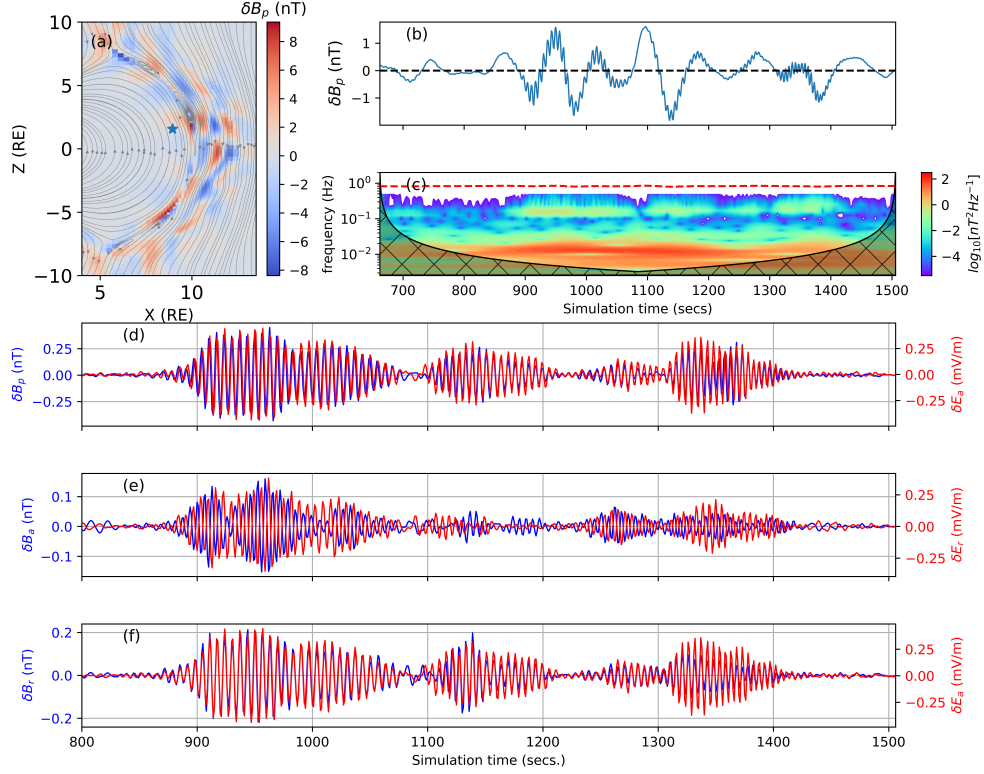


**Figure 1.** (a) variation of B in the parallel direction on  $Y = -3.5R_E$  plane at  $t = 956$  s. (b) its time evolution from a virtual spacecraft located at  $[x = 8.95, y = -3.5, z = 1.57]R_E$  the blue asterisk in (a), (c) Morlet wavelet transform of (b), shaded area is the cone of influence and the dashed red line is the local gyrofrequency. The lower three panels (d, e, and f) consist of polarization components (compressional, toroidal, and poloidal, respectively) of the magnetic field filtered in the Pc2 wave,  $[0.1, 0.5]$  Hz, frequency range.

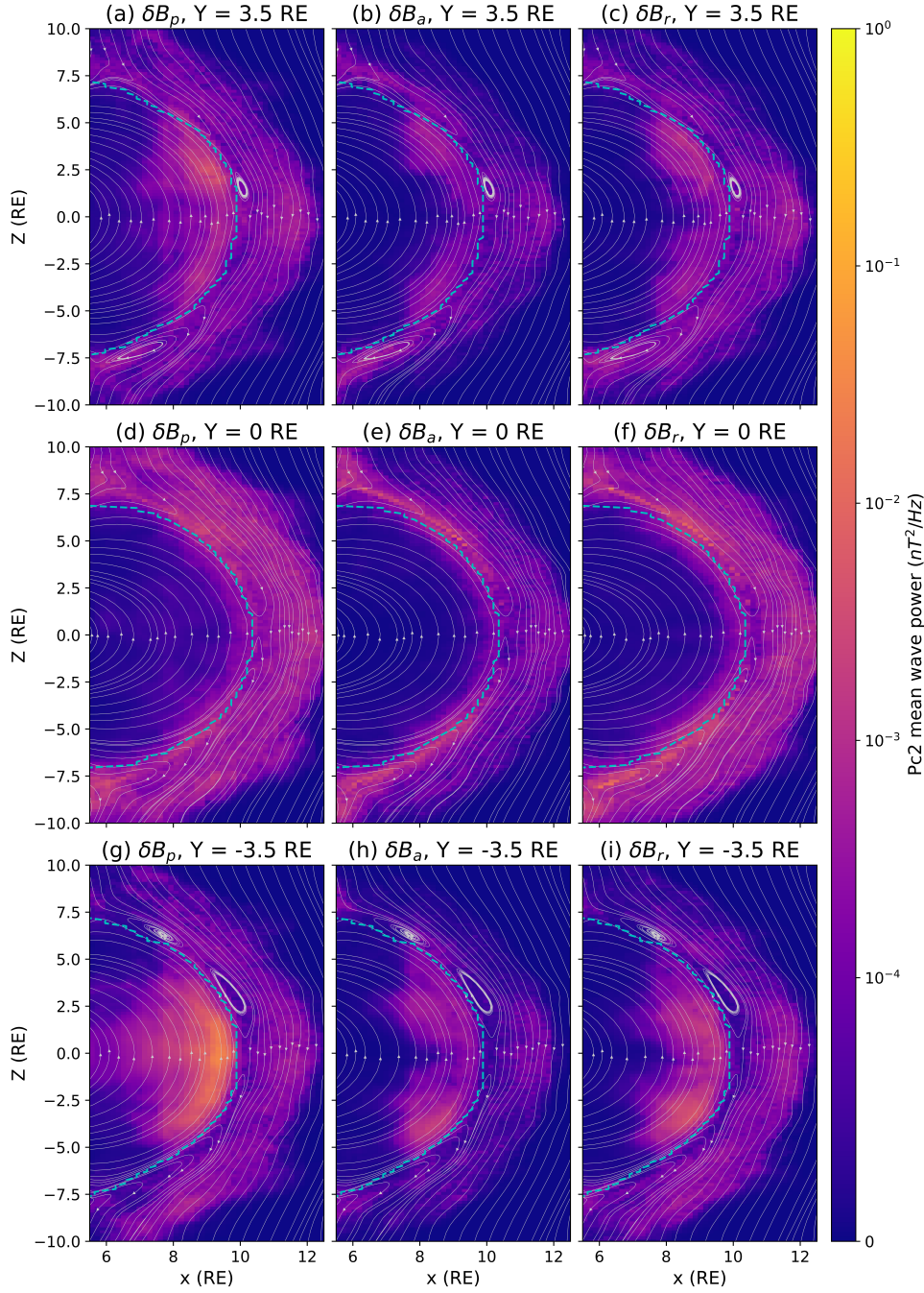


**Figure 2.** Spatial distribution of mean wave power in Pc2 range of compressional, toroidal, and poloidal components at the cross-sectional plane in the postnoon (top row), noon (mid row) and prenoon (bottom row) sectors, using the parallel, azimuthal, and radial component of the magnetic field. The cyan curve shows the approximate location of the magnetopause ( $\beta^* = 1.2$ ) according to Brenner et al. (2021). The light gray magnetic field lines represent the magnetosphere condition at  $t = 1112$  seconds into the simulation.

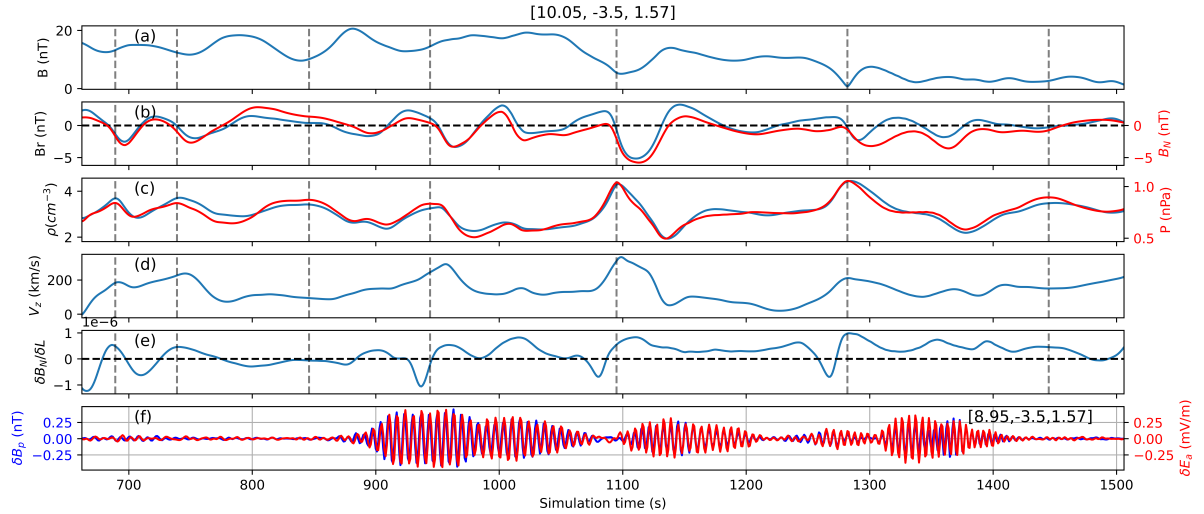


**Figure 3.** (a) Magnitude of magnetic field at the virtual spacecraft in the vicinity of the magnetopause at  $[x = 10.05, y = -3.5, z = 1.57]R_E$ , (b) radial and local normal N component of magnetic field, (c) proton density and pressure, (d) the z-component of proton velocity, and (e) the gradient of the local normal magnetic field in the local magnetic field direction. The vertical dashed lines show the time of FTEs at the virtual spacecraft location based on pressure peaks. The last panel shows the compressional ULF pulsation in the Pc2 frequency range from a virtual spacecraft at the same location as Figure 1 (a).

316 ship for Advanced Computing in Europe (PRACE) Tier-0 supercomputer infrastructure  
 317 in HLRS Stuttgart (project number PRACE-2019204998). Additional support came from  
 318 Academy of Finland Grants 339327, 335554, 347795, 345701, and 336805. The contri-  
 319 butions of M. Grandin (AERGELC'H project, Grant 338629), Y. Pfau-Kempf (KIMCHI  
 320 project, Grant 339756), L. Turc (UNTWINE project, Grant 322544), V. Tarvus (UN-  
 321 TWINE project, Grant 353197), and H. Zhou (RESSAC project, 3-year research Grant  
 322 2020–2022) were supported by the Academy of Finland and the University of Helsinki.  
 323 Wavelet software was provided by Grinsted et al. (2004), which is available at [http://](http://noc.ac.uk/using-science/crosswavelet-wavelet-coherence)  
 324 [noc.ac.uk/using-science/crosswavelet-wavelet-coherence](http://noc.ac.uk/using-science/crosswavelet-wavelet-coherence).

## 325 References

- 326 Akhavan-Tafti, M., Palmroth, M., Slavin, J. A., Battarbee, M., Ganse, U., Grandin,  
 327 M., ... Stawarz, J. E. (2020, 7). Comparative Analysis of the Vlasiator Sim-  
 328 ulations and MMS Observations of Multiple X-Line Reconnection and Flux  
 329 Transfer Events. *Journal of Geophysical Research: Space Physics*, 125(7),  
 330 e2019JA027410. doi: 10.1029/2019JA027410
- 331 Alho, M., Cozzani, G., Zaitsev, I., Kebede, F. T., Ganse, U., Battarbee, M., ...  
 332 Palmroth, M. (2023). Finding reconnection lines and flux rope axes via local  
 333 coordinates in global ion-kinetic magnetospheric simulations. *EGUsphere*,  
 334 2023, 1–24. doi: 10.5194/egusphere-2023-2300
- 335 Anderson, B. J., Erlandson, R. E., & Zanetti, L. J. (1992, 3). A statistical study  
 336 of Pc 1-2 magnetic pulsations in the equatorial magnetosphere: 1. Equatorial  
 337 occurrence distributions. *Journal of Geophysical Research: Space Physics*,  
 338 97(A3), 3075–3088. doi: 10.1029/91JA02706
- 339 Arnoldy, R. L., Engebretson, M. J., & Cahill, L. J. (1988, 2). Bursts of Pc 1-2 near  
 340 the ionospheric footprint of the cusp and their relationship to flux transfer

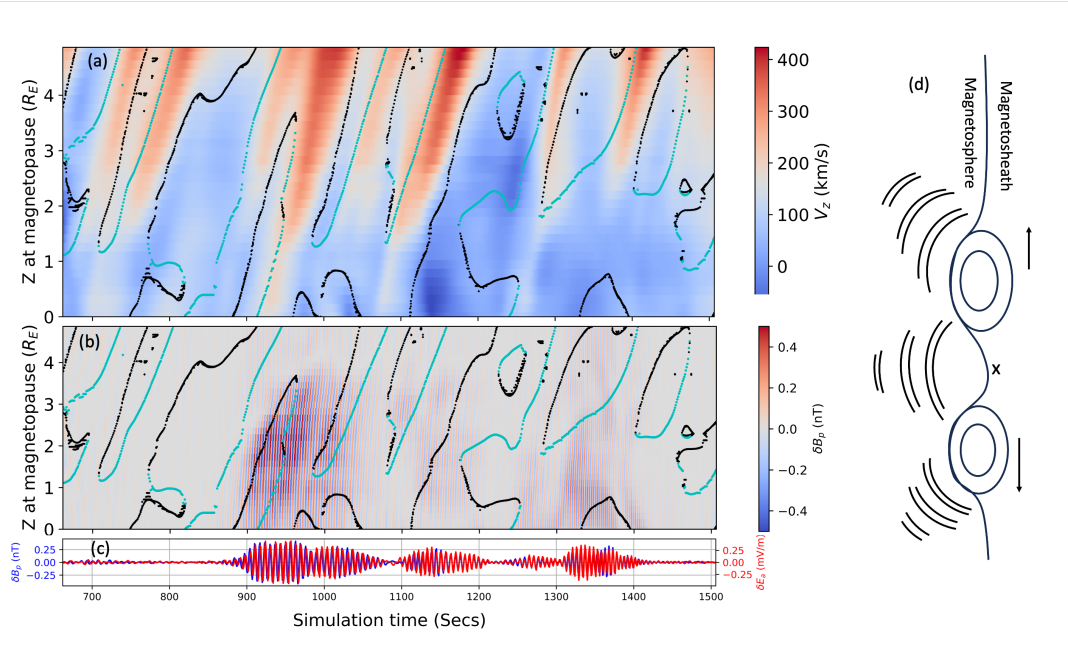


**Figure 4.** (a) A stacked plot showcasing the plasma bulk velocity from a curve along the Z-direction along the magnetopause surface, ranging from  $Z = 0 R_E$  to  $Z = 5 R_E$  on the plane  $Y = -3.5 R_E$ , (b) a similar stacked plot but for the Pc2 wave resulting from pulsations in the parallel component of the magnetic field, occurring on a surface parallel to the magnetopause and situated inside the magnetosphere including the blue star at  $Z = 1.57 R_E$  shown in Figure 1 (a), and (c) a replication of the panel as displayed in Figure 3 (f), (d) a cartoon illustrating different sources of waves discussed, as depicted in the accompanying video (Movie S1), X denotes the reconnection point. The contour lines in (a) and (b) are the X points (black) and O points (cyan).

- 341 events. *Journal of Geophysical Research: Space Physics*, 93(A2), 1007–1016.  
 342 doi: 10.1029/JA093IA02P01007
- 343 Battarbee, M., Hannuksela, O. A., Pfau-Kempf, Y., Alftan, S. v., Ganse, U., Jarvi-  
 344 nen, R., ... Grandin, M. (2021, 1). fmihpc/analysator: v0.9.  
 345 doi: 10.5281/ZENODO.4462515
- 346 Bentley, S. N., Watt, C. E., Owens, M. J., & Rae, I. J. (2018, 4). ULF Wave Activ-  
 347 ity in the Magnetosphere: Resolving Solar Wind Interdependencies to Identify  
 348 Driving Mechanisms. *Journal of Geophysical Research: Space Physics*, 123(4),  
 349 2745–2771. doi: 10.1002/2017JA024740
- 350 Brenner, A., Pulkkinen, T. I., Al Shidi, Q., & Toth, G. (2021, 10). Stormtime  
 351 Energetics: Energy Transport Across the Magnetopause in a Global MHD  
 352 Simulation. *Frontiers in Astronomy and Space Sciences*, 8, 180. doi:  
 353 10.3389/FSPAS.2021.756732/BIBTEX
- 354 Fear, R. C., Milan, S. E., Fazakerley, A. N., Lucek, E. A., Cowley, S. W., & Dan-  
 355 douras, I. (2008, 8). The azimuthal extent of three flux transfer events. *An-  
 356 nales Geophysicae*, 26(8), 2353–2369. Retrieved from [www.ann-geophys.net/  
 357 26/2353/2008/](http://www.ann-geophys.net/26/2353/2008/) doi: 10.5194/ANGE0-26-2353-2008
- 358 Ganse, U., Koskela, T., Battarbee, M., Pfau-Kempf, Y., Papadakis, K., Alho, M.,  
 359 ... Palmroth, M. (2023, 4). Enabling technology for global 3D + 3V hybrid-  
 360 Vlasov simulations of near-Earth space. *Physics of Plasmas*, 30(4), 42902.  
 361 Retrieved from [https://pubs.aip.org/aip/pop/article/30/4/042902/  
 362 2878614/Enabling-technology-for-global-3D-3V-hybrid-Vlasov](https://pubs.aip.org/aip/pop/article/30/4/042902/2878614/Enabling-technology-for-global-3D-3V-hybrid-Vlasov) doi:  
 363 10.1063/5.0134387/2878614
- 364 Gillis, E. J., Rijnbeek, R., Kling, R., Speiser, T. W., & Fritz, T. A. (1987, 6).  
 365 Do flux transfer events cause long-period micropulsations in the dayside  
 366 magnetosphere? *Journal of Geophysical Research*, 92(A6), 5820. doi:  
 367 10.1029/JA092iA06p05820
- 368 Glasmeier, K., Lester, M., Mier-Jedrzejowicz, W., Green, C., Rostoker, G., Orr, D.,  
 369 ... Amata, E. (1984, 8). Pc5 pulsations and their possible source mecha-  
 370 nisms: a case study. *Journal of Geophysics*, 55(1), 108–119. Retrieved from  
 371 <https://journal.geophysicsjournal.com/JofG/article/view/205>
- 372 Grandin, M., Luttikhuis, T., Battarbee, M., Cozzani, G., Zhou, H., Turc, L., ...  
 373 Palmroth, M. (2023). First 3D hybrid-Vlasov global simulation of auroral  
 374 proton precipitation and comparison with satellite observations. *Journal of  
 375 Space Weather and Space Climate*, 13, 20. doi: 10.1051/SWSC/2023017
- 376 Grinsted, A., Moore, J. C., & Jevrejeva, S. (2004, 11). Application of the cross  
 377 wavelet transform and wavelet coherence to geophysical time series. *Nonlinear  
 378 Processes in Geophysics*, 11(5/6), 561–566. doi: 10.5194/NPG-11-561-2004
- 379 Grison, B., Santolík, O., Lukačević, J., & Usanova, M. E. (2021, 2). Occurrence of  
 380 EMIC Waves in the Magnetosphere According to Their Distance to the Mag-  
 381 netopause. *Geophysical Research Letters*, 48(3). doi: 10.1029/2020GL090921
- 382 Hasegawa, H., Sonnerup, B. U., Owen, C. J., Klecker, B., Paschmann, G., Balogh,  
 383 A., & Rème, H. (2006, 3). The structure of flux transfer events recov-  
 384 ered from Cluster data. *Annales Geophysicae*, 24(2), 603–618. doi:  
 385 10.5194/ANGE0-24-603-2006
- 386 Hasegawa, H., Wang, J., Dunlop, M. W., Pu, Z. Y., Zhang, Q. H., Lavraud, B., ...  
 387 Bogdanova, Y. V. (2010, 8). Evidence for a flux transfer event generated  
 388 by multiple X-line reconnection at the magnetopause. *Geophysical Research  
 389 Letters*, 37(16). doi: 10.1029/2010GL044219
- 390 Hoilijoki, S., Ganse, U., Pfau-Kempf, Y., Cassak, P. A., Walsh, B. M., Hietala,  
 391 H., ... Palmroth, M. (2017, 3). Reconnection rates and X line motion  
 392 at the magnetopause: Global 2D-3V hybrid-Vlasov simulation results.  
 393 *Journal of Geophysical Research: Space Physics*, 122(3), 2877–2888. doi:  
 394 10.1002/2016JA023709

- 395 Hwang, K. J. (2015). Magnetopause Waves Controlling the Dynamics of Earth's  
396 Magnetosphere. *Journal of Astronomy and Space Sciences*, *32*(1), 1–11. doi:  
397 10.5140/JASS.2015.32.1.1
- 398 Hwang, K. J., & Sibeck, D. G. (2016, 2). Role of Low-Frequency Bound-  
399 ary Waves in the Dynamics of the Dayside Magnetopause and the Inner  
400 Magnetosphere. *Low-Frequency Waves in Space Plasmas*, 213–239. doi:  
401 10.1002/9781119055006.CH13
- 402 Kavosi, S., & Raeder, J. (2015, 5). Ubiquity of Kelvin–Helmholtz waves at Earth's  
403 magnetopause. *Nature Communications 2015 6:1*, *6*(1), 1–6. doi: 10.1038/  
404 ncomms8019
- 405 Kokubun, S., Yamamoto, T., Hayashi, K., Oguti, T., & Egeland, A. (1988). Im-  
406 pulsive Pi Bursts Associated with Poleward Moving Auroras Near the Polar  
407 Cusp. *Journal of geomagnetism and geoelectricity*, *40*(5), 537–551. doi:  
408 10.5636/JGG.40.537
- 409 Kronberg, E. A., Gorman, J., Nykyri, K., Smirnov, A. G., Gjerloev, J. W., Grig-  
410 orenko, E. E., ... Friel, M. (2021, 12). Kelvin-Helmholtz Instability Associated  
411 With Reconnection and Ultra Low Frequency Waves at the Ground: A Case  
412 Study. *Frontiers in Physics*, *9*, 738988. doi: 10.3389/FPHY.2021.738988/  
413 BIBTEX
- 414 Lee, D.-H., & Lysak, R. L. (1989, 12). Magnetospheric ULF wave coupling in the  
415 dipole model: The impulsive excitation. *Journal of Geophysical Research*,  
416 *94*(A12), 17097. doi: 10.1029/JA094iA12p17097
- 417 Liu, J., Angelopoulos, V., Sibeck, D., Phan, T., Pu, Z. Y., McFadden, J., ... Auster,  
418 H. U. (2008, 9). THEMIS observations of the dayside traveling compression re-  
419 gion and flows surrounding flux transfer events. *Geophysical Research Letters*,  
420 *35*(17). doi: 10.1029/2008GL033673
- 421 Liu, Y. H., Fraser, B. J., & Menk, F. M. (2012, 9). Pc2 EMIC waves generated high  
422 off the equator in the dayside outer magnetosphere. *Geophysical Research Let-  
423 ters*, *39*(17). doi: 10.1029/2012GL053082
- 424 McPherron, R. L. (2005, 9). Magnetic pulsations: Their sources and relation to solar  
425 wind and geomagnetic activity. *Surveys in Geophysics*, *26*(5), 545–592. doi: 10  
426 .1007/S10712-005-1758-7/METRICS
- 427 Menk, F. W., Menk, & W., F. (2011). Magnetospheric ULF Waves: A Review.  
428 *dyma*, *3*, 223–256. doi: 10.1007/978-94-007-0501-2{\\_}13
- 429 Palmroth, M., Archer, M., Vainio, R., Hietala, H., Pfau-Kempf, Y., Hoilijoki, S.,  
430 ... Eastwood, J. P. (2015, 10). ULF foreshock under radial IMF: THEMIS  
431 observations and global kinetic simulation Vlasiator results compared. *Jour-  
432 nal of Geophysical Research: Space Physics*, *120*(10), 8782–8798. doi:  
433 10.1002/2015JA021526
- 434 Palmroth, M., Ganse, U., Yann Pfau-Kempf, , Battarbee, M., Turc, L., Brito, T.,  
435 ... Sebastian Von Alfthan, (2018, 8). Vlasov methods in space physics and  
436 astrophysics. *Living Reviews in Computational Astrophysics 2018 4:1*, *4*(1),  
437 1–54. doi: 10.1007/S41115-018-0003-2
- 438 Palmroth, M., Pulkkinen, T. I., Ganse, U., Pfau-Kempf, Y., Koskela, T., Zaitsev, I.,  
439 ... Nakamura, R. (2023, 6). Magnetotail plasma eruptions driven by magnetic  
440 reconnection and kinetic instabilities. *Nature Geoscience 2023 16:7*, *16*(7),  
441 570–576. doi: 10.1038/s41561-023-01206-2
- 442 Palmroth, M., Raptis, S., Suni, J., Karlsson, T., Turc, L., Johlander, A., ... Os-  
443 mane, A. (2021, 3). Magnetosheath jet evolution as a function of lifetime:  
444 Global hybrid-Vlasov simulations compared to MMS observations. *Annales  
445 Geophysicae*, *39*(2), 289–308. doi: 10.5194/ANGE0-39-289-2021
- 446 Paschmann, G., Haerendel, G., Papamastorakis, I., Sckopke, N., Bame, S. J.,  
447 Gosling, J. T., & Russell, C. T. (1982). Plasma and magnetic field charac-  
448 teristics of magnetic flux transfer events. *Journal of Geophysical Research*,  
449 *87*(A4), 2159. doi: 10.1029/JA087IA04P02159

- 450 Pfau-Kempf, Y., Alfthan, S. v., Ganse, U., Sandroos, A., Battarbee, M., Koskela,  
451 T., ... Alho, M. (2022, 6). fmi-hpc/vlasiator: Vlasiator 5.2.1. Retrieved from  
452 <https://zenodo.org/record/6782211> doi: 10.5281/ZENODO.6782211
- 453 Pfau-Kempf, Y., Battarbee, M., Ganse, U., Hoilijoki, S., Turc, L., von Alfthan, S.,  
454 ... Palmroth, M. (2018, 5). On the importance of spatial and velocity resolu-  
455 tion in the hybrid-Vlasov modeling of collisionless shocks. *Frontiers in Physics*,  
456 6(MAY), 44. doi: 10.3389/FPHY.2018.00044/BIBTEX
- 457 Pfau-Kempf, Y., Hietala, H., Milan, S. E., Juusola, L., Hoilijoki, S., Ganse,  
458 U., ... Palmroth, M. (2016). Evidence for transient, local ion fore-  
459 shocks caused by dayside magnetopause reconnection. , 34, 943–959. doi:  
460 10.5194/angeo-34-943-2016
- 461 Pfau-Kempf, Y., Palmroth, M., Johlander, A., Turc, L., Alho, M., Battarbee, M.,  
462 ... Ganse, U. (2020, 9). Hybrid-Vlasov modeling of three-dimensional day-  
463 side magnetopause reconnection. *Physics of Plasmas*, 27(9), 092903. doi:  
464 10.1063/5.0020685/5.0020685.MM.ORIGINAL.V1.MP4
- 465 Regi, M., Del Corpo, A., & De Laetis, M. (2017, 1). The use of the empiri-  
466 cal mode decomposition for the identification of mean field aligned reference  
467 frames. *Annals of Geophysics*, 59(6), G0651. Retrieved from [https://](https://www.annalsofgeophysics.eu/index.php/annals/article/view/7067)  
468 [www.annalsofgeophysics.eu/index.php/annals/article/view/7067](https://www.annalsofgeophysics.eu/index.php/annals/article/view/7067) doi:  
469 10.4401/ag-7067
- 470 Remya, B., Sibeck, D. G., Halford, A. J., Murphy, K. R., Reeves, G. D., Singer,  
471 H. J., ... Thaller, S. A. (2018, 6). Ion Injection Triggered EMIC Waves in  
472 the Earth's Magnetosphere. *Journal of Geophysical Research: Space Physics*,  
473 123(6), 4921–4938. doi: 10.1029/2018JA025354
- 474 Ripoll, J., Claudepierre, S. G., Ukhorskiy, A. Y., Colpitts, C., Li, X., Fennell,  
475 J. F., & Crabtree, C. (2020, 5). Particle Dynamics in the Earth's Ra-  
476 diation Belts: Review of Current Research and Open Questions. *Jour-*  
477 *nal of Geophysical Research: Space Physics*, 125(5). Retrieved from  
478 <https://onlinelibrary.wiley.com/doi/abs/10.1029/2019JA026735> doi:  
479 10.1029/2019JA026735
- 480 Russell, C. T., & Elphic, R. C. (1979). ISEE observations of flux transfer events at  
481 the dayside magnetopause. *Geophysical Research Letters*, 6(1), 33–36. doi: 10  
482 .1029/GL006I001P00033
- 483 Sun, T. R., Tang, B. B., Wang, C., Guo, X. C., & Wang, Y. (2019, 4). Large-Scale  
484 Characteristics of Flux Transfer Events on the Dayside Magnetopause. *Jour-*  
485 *nal of Geophysical Research: Space Physics*, 124(4), 2425–2434. doi: 10.1029/  
486 2018JA026395
- 487 Takahashi, K., Turc, L., Kilpua, E., Takahashi, N., Dimmock, A., Kajdic, P.,  
488 ... Battarbee, M. (2021, 2). Propagation of Ultralow-Frequency Waves  
489 from the Ion Foreshock into the Magnetosphere During the Passage of a  
490 Magnetic Cloud. *Journal of Geophysical Research: Space Physics*, 126(2),  
491 e2020JA028474. doi: 10.1029/2020JA028474
- 492 Tan, B., Lin, Y., Perez, J. D., & Wang, X. Y. (2011). Global-scale hybrid simulation  
493 of dayside magnetic reconnection under southward IMF: Structure and evolu-  
494 tion of reconnection. *J. Geophys. Res.*, 116, 2206. doi: 10.1029/2010JA015580
- 495 Teh, W. L., Nakamura, T. K., Nakamura, R., Baumjohann, W., Russell, C. T., Pol-  
496 lock, C., ... Giles, B. L. (2017, 2). Evolution of a typical ion-scale magnetic  
497 flux rope caused by thermal pressure enhancement. *Journal of Geophysical*  
498 *Research: Space Physics*, 122(2), 2040–2050. doi: 10.1002/2016JA023777
- 499 Tetrack, S. S., Engebretson, M. J., Posch, J. L., Olson, C. N., Smith, C. W., Den-  
500 ton, R. E., ... Fennell, J. F. (2017, 4). Location of intense electromagnetic  
501 ion cyclotron (EMIC) wave events relative to the plasmopause: Van Allen  
502 Probes observations. *Journal of Geophysical Research: Space Physics*, 122(4),  
503 4064–4088. doi: 10.1002/2016JA023392

- 504 Torrence, C., & Compo, P. (1998). A practical guide to wavelet analysis. *Bulletin of*  
505 *the American Meteorological Society*, 61–78. doi: 10.1175/1520-0477(1998)079
- 506 Trattner, K. J., Petrinec, S. M., & Fuselier, S. A. (2021, 3). The Location of Mag-  
507 netic Reconnection at Earth’s Magnetopause. *Space Science Reviews 2021*  
508 *217:3*, 217(3), 1–47. doi: 10.1007/S11214-021-00817-8
- 509 Turc, L., Roberts, O. W., Verscharen, D., Dimmock, A. P., Kajdič, P., Palm-  
510 roth, M., . . . Ganse, U. (2022, 12). Transmission of foreshock waves  
511 through Earth’s bow shock. *Nature Physics 2022 19:1*, 19(1), 78–86. doi:  
512 10.1038/s41567-022-01837-z
- 513 Turc, L., Zhou, H., Tarvus, V., Ala-Lahti, M., Battarbee, M., Pfau-Kempf, Y., . . .  
514 Palmroth, M. (2022, 9). A global view of Pc3 wave activity in near-Earth  
515 space: Results from hybrid-Vlasov simulations. *Frontiers in Astronomy and*  
516 *Space Sciences*, 9, 989369. doi: 10.3389/FSPAS.2022.989369/BIBTEX
- 517 Usanova, M. E., Mann, I. R., Bortnik, J., Shao, L., & Angelopoulos, V. (2012,  
518 10). THEMIS observations of electromagnetic ion cyclotron wave oc-  
519 currence: Dependence on AE, SYMH, and solar wind dynamic pressure.  
520 *Journal of Geophysical Research: Space Physics*, 117(A10), 10218. doi:  
521 10.1029/2012JA018049
- 522 Von Althaus, S., Pokhotelov, D., Kempf, Y., Hoilijoki, S., Honkonen, I., Sandroos,  
523 A., & Palmroth, M. (2014, 12). Vlasiator: First global hybrid-Vlasov simu-  
524 lations of Earth’s foreshock and magnetosheath. *Journal of Atmospheric and*  
525 *Solar-Terrestrial Physics*, 120, 24–35. doi: 10.1016/J.JASTP.2014.08.012
- 526 Walsh, B. M., Komar, C. M., & Pfau-Kempf, Y. (2017, 4). Spacecraft measure-  
527 ments constraining the spatial extent of a magnetopause reconnection X line.  
528 *Geophysical Research Letters*, 44(7), 3038–3046. doi: 10.1002/2017GL073379
- 529 Wang, C. P., Thorne, R., Liu, T. Z., Hartinger, M. D., Nagai, T., Angelopoulos,  
530 V., . . . Spence, H. E. (2017, 5). A multispacecraft event study of Pc5  
531 ultralow-frequency waves in the magnetosphere and their external drivers.  
532 *Journal of Geophysical Research: Space Physics*, 122(5), 5132–5147. doi:  
533 10.1002/2016JA023610
- 534 Wang, H., Lin, Y., Wang, X., & Guo, Z. (2019, 7). Generation of kinetic Alfvén  
535 waves in dayside magnetopause reconnection: A 3-D global-scale hybrid simu-  
536 lation. *Physics of Plasmas*, 26(7), 072102. doi: 10.1063/1.5092561
- 537 Yagodkina, O. I., & Vorobjev, V. G. (1997). Daytime high-latitude pulsations  
538 associated with solar wind dynamic pressure impulses and flux transfer  
539 events. *Journal of Geophysical Research: Space Physics*, 102(A1), 57–67.  
540 doi: 10.1029/96JA01273
- 541 Zhang, H., Kivelson, M. G., Angelopoulos, V., Khurana, K. K., Walker, R. J., Jia,  
542 Y. D., . . . Auster, H. U. (2011, 8). Flow vortices associated with flux transfer  
543 events moving along the magnetopause: Observations and an MHD simula-  
544 tion. *Journal of Geophysical Research: Space Physics*, 116(A8), 8202. Re-  
545 trieved from [https://agupubs.onlinelibrary.wiley.com/doi/10.1029/](https://agupubs.onlinelibrary.wiley.com/doi/10.1029/2011JA016500)  
546 [2011JA016500](https://agupubs.onlinelibrary.wiley.com/doi/10.1029/2011JA016500) doi: 10.1029/2011JA016500
- 547 Zong, Q., Rankin, ., & Zhou, . (2017, 11). The interaction of ultra-low-frequency  
548 pc3-5 waves with charged particles in Earth’s magnetosphere. *Reviews of Mod-  
549 ern Plasma Physics 2017 1:1*, 1(1), 1–90. doi: 10.1007/S41614-017-0011-4

Figure1.

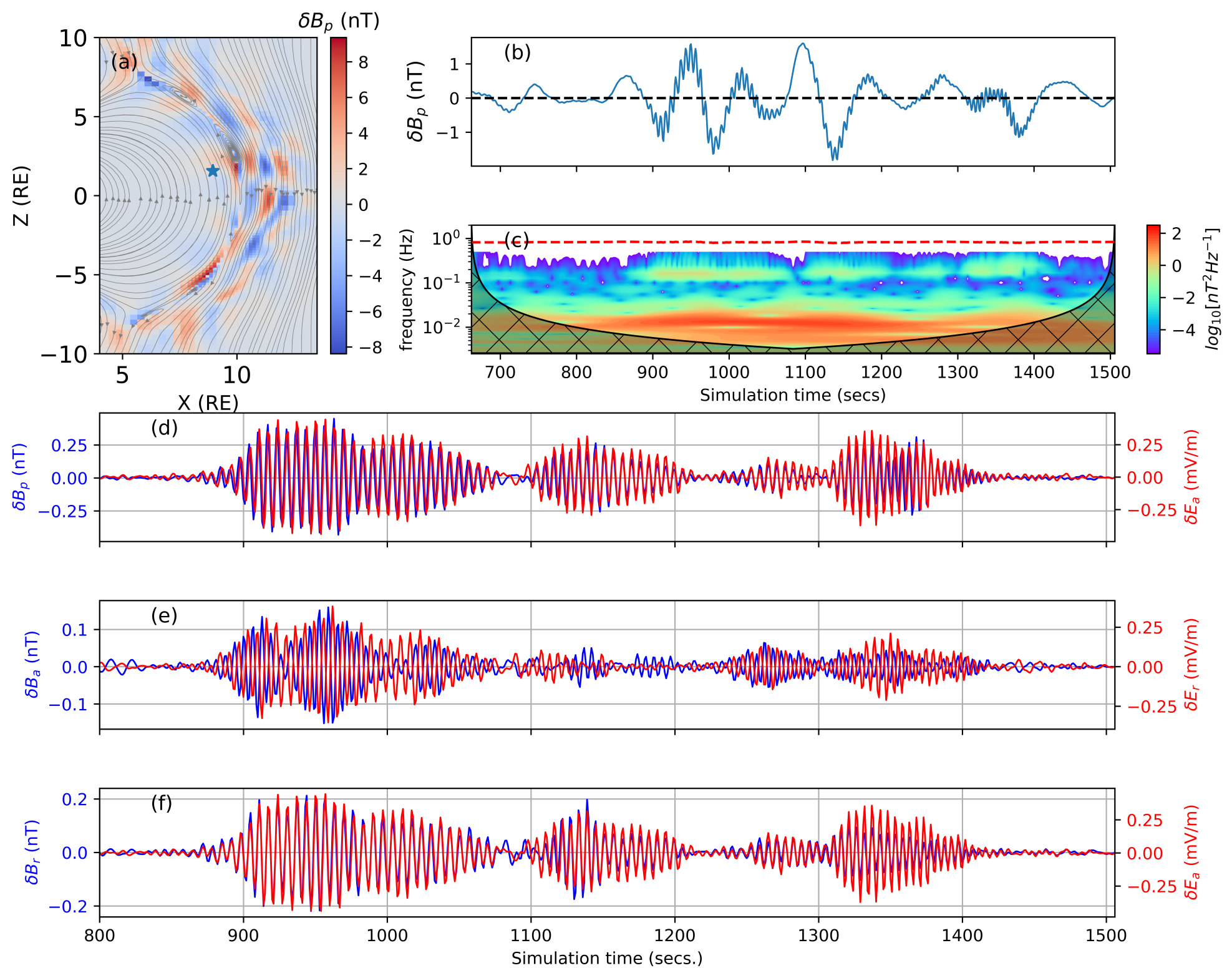


Figure2.

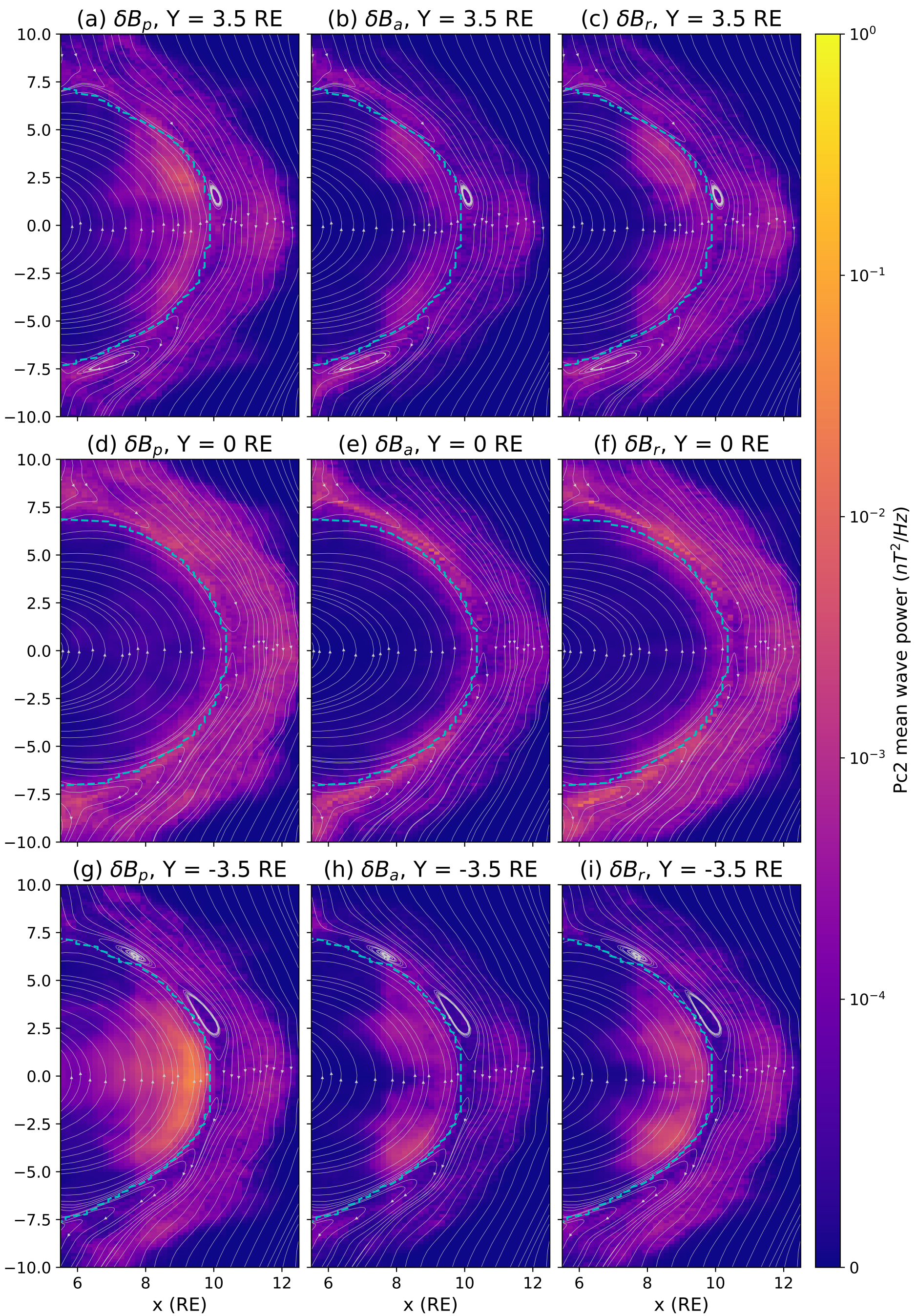


Figure3.

[10.05, -3.5, 1.57]

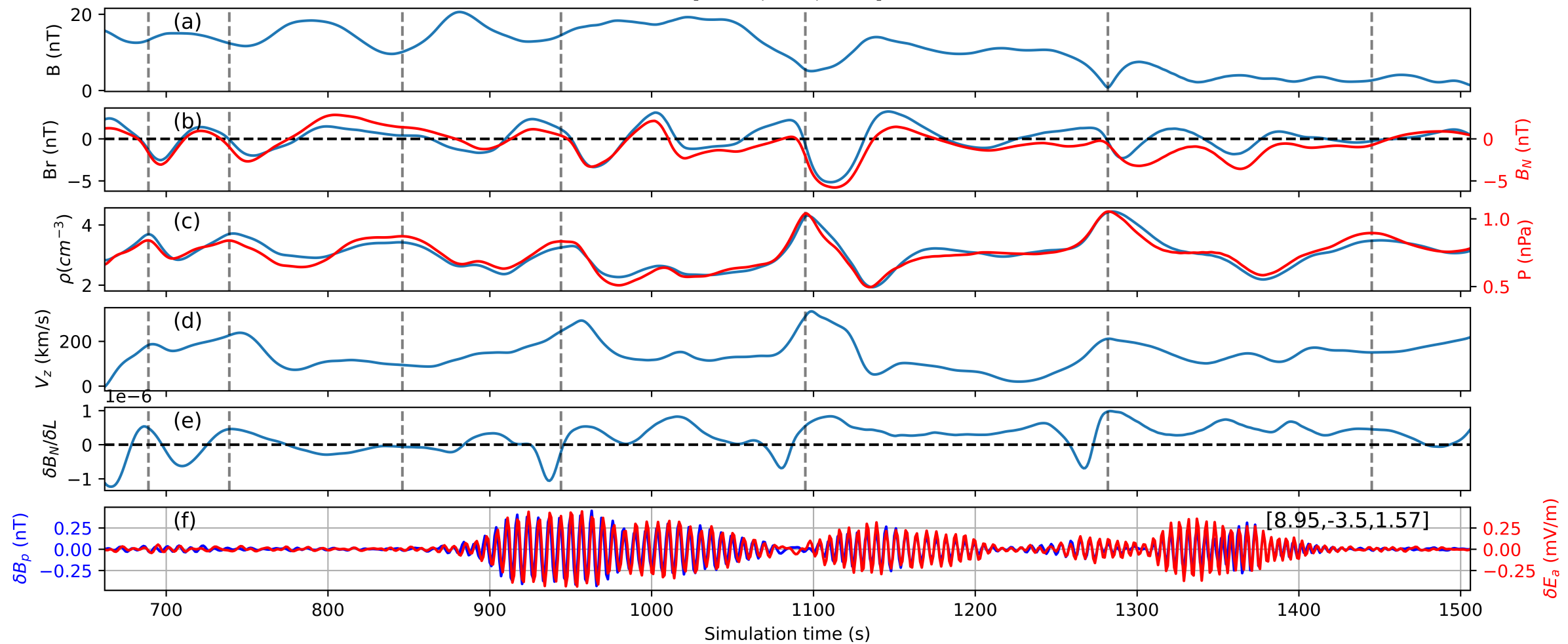


Figure4.

